LORENTZ FORCE TYPE INTEGRATED MOTOR-BEARING SYSTEM IN DUAL ROTOR DISK CONFIGURATION

Sung-Ho Park
Center for Noise and Vibration Control (NOVIC), KAIST, Science town, Daejeon, 305-701, Korea
shpark@cwllab.kaist.ac.kr

Chong-Won Lee
Center for Noise and Vibration Control (NOVIC), KAIST, Science town, Daejeon, 305-701, Korea
cwlee@novic.kaist.ac.kr

ABSTRACT

This paper proposes a generalized principle for the generation of torque and radial force in integrated motor-bearing systems using Lorentz force. The derived constraints lead to various feasible combinations of design parameters. Dual rotor disk configuration with a coreless stator is also proposed. It induces no negative stiffness, which is useful for the system stability and robustness to the tilting motion of the rotor. The test rig is developed for 5 and 6 windings with an 8-pole rotor and operated successfully employing a simple PD-like controller.

NOMENCLATURE

A	Magnitude of motoring current
B	Peak of air gap flux density generated by rotor magnets
C	Magnitude of radial force current
k	Number of turns per concentrated winding
l	Effective length of winding part crossing the flux
M	Number of pole pairs for motoring current ($M \geq 1$)
N	Number of pole pairs for radial force current ($N \geq 1$)
$\mathcal{N}$	Set of natural numbers
Q	Number of pole pairs for rotor permanent magnets
r	Effective radius of stator windings
t	Time
W	Number of windings ($W \geq 5$)
2α	Winding pitch angle
η	Winding angular interval
θ	Angular coordinate fixed at stator
ϕ	Phase shift of radial force control current
ψ	Phase shift of motoring current
ω	AC current frequency [rad/sec]

INTRODUCTION

Since one and half decades ago, extensive works have been carried out in order to develop various kinds of integrated motor-bearing systems [1], such as induction type, permanent magnet type, homopolar type, reluctance type, etc. Most of them, however, have the design principles based on the use of Maxwell force for the position control of rotor. In recent years, new integrated motor-bearing systems employing Lorentz force for the rotor position regulation as well as motoring have been proposed [2-5]. Introducing Lorentz force in the stabilization of rotor can make the analysis and design of the system easy due to its bi-directional and good linear properties. In addition, it allows the rotor permanent magnets to have sufficient thickness for preventing demagnetization problem. Han, et al. [2] developed such a Lorentz force type integrated motor-bearing system in a disk shape. It necessitates a complex frequency demodulation skill with two stator disks to avoid singularity in calculating control inputs. Stephens, et al. [3] proposed the system applying 3 phase BLDC motors as 4 magnetic actuators. The magnitude unbalance of facing motor current can control the rotor radial position. This concept is easy to understand intuitively, but it requires 4 units of 3 phase current drivers and 16-pole rotor. Okada, et al. [4] and Kim, et al. [5] introduced the principle in which the phase angle of radial force current determines the force direction. They developed prototypes with 6 concentrated common stator windings driven by separated amplifiers. Though the experiments attained a successful operation, the theory applies only for a specific number of poles and winding distribution.

In this paper, extended design conditions for Lorentz force type integrated motor-bearing systems with generalized parameters are presented. The constraints for arrangement of permanent magnets and winding distribution are derived based on the use of common windings for both torque and position control. Typical feasible combinations of design parameters

satisfying the conditions are presented. The disk type or axial flux motor is an attractive alternative to the cylindrical radial flux motor due to its short frame, compact construction, and high power density. This work suggests the composition of two rotor disks and a coreless stator for the experimental prototypes of integrated motor-bearing system based on the principle. A pair of rotor disks is located at both sides of the stator disk like a sandwich. Coreless stator no longer needs a difficult spiral lamination and slotting technique. It leads to relatively small winding inductance. It can also eliminate such troubles as slot harmonics, iron loss, eddy current effect, hysteresis, and magnetic saturation. Most of all, it brings no negative stiffness in the radial direction, which makes the system originally stable and robust to tilting motion of the rotor disks. The experiment was performed for 5 and 6 stator windings with an 8-pole rotor. These two combinations have been selected such that overlapping or crossing of adjacent windings can be avoided for the minimum number of rotor permanent magnets.

DESIGN PRINCIPLE

Let us consider the W equi-spaced concentrated windings along the periphery of the stator as shown in Fig. 1. The positive sign is assigned to the magnetic flux coming out of the page, and to the effective current running from the center of the stator to the outer radial direction. Under that sign convention, the stator will deliver a positive torque in the counter-clockwise direction. For simplicity of analysis, assume that the magnetic flux density generated by the rotor permanent magnets takes a sinusoidal waveform of

$$B_R = B\cos(\omega t - Q\theta) \tag{1}$$

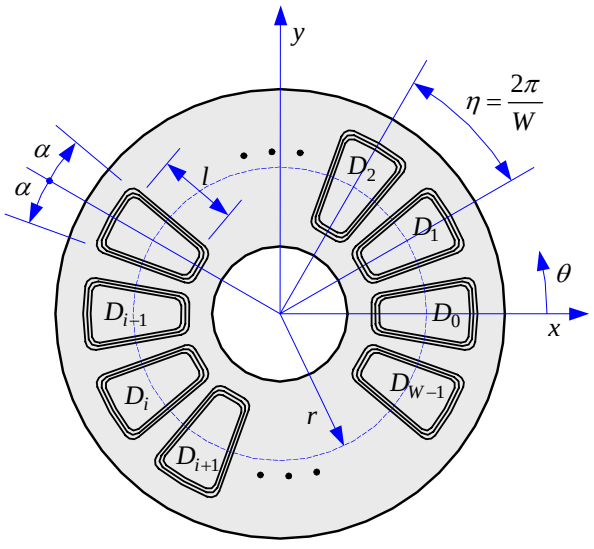

FIGURE 1: Coordinates and winding distribution

where B is the amplitude of the flux density, ω is the AC circular frequency, Q is the number of pole pairs of the rotor permanent magnets and θ is the angular coordinate. Now consider the currents for motoring torque given in the form of

$$I_i^M = A\cos(\omega t + \psi - M\eta i) \quad i = 0, 1, \cdots, W-1 \tag{2}$$

where A is the magnitude of the current, ψ is the phase shift, M denotes the number of pole pairs for motoring current in the stator windings, and the angular spacing of the windings η is defined as

$$\eta \equiv \frac{2\pi}{W} \tag{3}$$

The stator winding distribution can be represented by using Dirac's delta function as

$$\begin{aligned} D_i &= k\delta(\theta - \eta i + \alpha) - k\delta(\theta - \eta i - \alpha) \\ & i = 0, 1, \cdots, W-1 \end{aligned} \tag{4}$$

where k is the number of turns in a concentrated winding and 2α is the winding pitch angle. Then the motoring torque produced by these currents can be obtained, using Lorentz law, as

$$\begin{aligned} T &= \sum_{i=0}^{W-1} rl \int_0^{2\pi} B_R I_i^M D_i d\theta \\ &= ABkrl\sin(Q\alpha)\left\{\sum_{i=0}^{W-1}\sin(\psi + (Q-M)\eta i)\right. \\ &\qquad \left. - \sum_{i=0}^{W-1}\sin(2\omega t + \psi - (Q+M)\eta i)\right\} \end{aligned} \tag{5}$$

Thus, the conditions for the torque to be a nonzero constant, regardless of the rotational speed of the rotor become

$$\begin{aligned} (Q+M)\eta &\neq 2m\pi \\ (Q-M)\eta &= 2n\pi \end{aligned} \tag{6}$$

where m and n are arbitrary integers. In other words, the number of pole pairs Q for the rotor permanent magnets and the number of pole pairs M for the motoring current should be determined so that they satisfy the relation, for the number of windings W, given by

$$\begin{aligned} Q &= M + nW \\ \frac{2M}{W} &\notin \mathcal{N} \end{aligned} \tag{7}$$

Equation (7) implies that the phase difference, $M\eta$ in equation (2), should be restricted to a proper fraction of π so that all motoring currents are not given in phase or out of phase of the reference state corresponding to, say, i = 0. It also means that (Q – M) should be an integer

multiple of *W*. Note, however, that *Q*, physically a natural number, can take a negative integer, since equation (1) still holds for –*Q*, which is equivalent to reversal of the sign convention for θ. For a negative integer value of *Q*, the torque direction will also be reversed so that the rotor will rotate clockwise. Substituting equation (7) into equation (5), we obtain

$$T = WABkrl \sin(Q\alpha)\sin\psi \tag{8}$$

implying that the motoring torque is proportional to the number of windings, the magnitudes of the motoring current and the magnetic flux, the number of turns, and the effective length of the winding. It suggests that we can control the system like a standard synchronous AC motor by adjusting the phase shift ψ as its torque angle. In addition, the torque attains its maximum value when the winding pitch angle 2α is tuned to the pitch angle of the rotor permanent magnets. The relation between the rotor speed N_S in rpm and the motoring current frequency *f* in Hz can be written as

$$N_S = \frac{60f}{Q} \quad \text{[RPM]} \tag{9}$$

where $\omega = 2\pi f$.

Similarly to the previous procedure for motoring torque generation, consider the currents for the radial control force in the form of

$$I_i^C = C\cos(\omega t + \phi - N\eta i) \quad i = 0, 1, \cdots, W-1 \tag{10}$$

where *C* is the magnitude of the current, ϕ is the phase shift, and *N* denotes the number of pole pairs for radial force control current in the stator windings, which should be, of course, different from *M*. Applying these currents to the windings represented by equation (4), we obtain the expressions for the radial control forces in the *x* and *y* directions as

$$\begin{aligned} F_x = -\sum_{i=0}^{W-1} l\int_0^{2\pi} B_R I_i^C D_i \sin\theta\, d\theta = \frac{1}{2}BCkl \times \\ \Big\{ \sin((Q+1)\alpha)\sum_{i=0}^{W-1}\cos(\phi + (Q-N+1)\eta i) \\ + \sin((Q+1)\alpha)\sum_{i=0}^{W-1}\cos(2\omega t + \phi - (Q+N+1)\eta i) \\ - \sin((Q-1)\alpha)\sum_{i=0}^{W-1}\cos(\phi + (Q-N-1)\eta i) \\ - \sin((Q-1)\alpha)\sum_{i=0}^{W-1}\cos(2\omega t + \phi - (Q+N-1)\eta i) \Big\} \end{aligned} \tag{11}$$

$$\begin{aligned} F_y = \sum_{i=0}^{W-1} l\int_0^{2\pi} B_R I_i^C D_i \cos\theta\, d\theta = \frac{1}{2}BCkl \times \\ \Big\{ \sin((Q+1)\alpha)\sum_{i=0}^{W-1}\sin(\phi + (Q-N+1)\eta i) \\ - \sin((Q+1)\alpha)\sum_{i=0}^{W-1}\sin(2\omega t + \phi - (Q+N+1)\eta i) \\ + \sin((Q-1)\alpha)\sum_{i=0}^{W-1}\sin(\phi + (Q-N-1)\eta i) \\ - \sin((Q-1)\alpha)\sum_{i=0}^{W-1}\sin(2\omega t + \phi - (Q+N-1)\eta i) \Big\} \end{aligned} \tag{12}$$

Eliminating the dependent terms upon ωt , we derive the conditions for generation of a stable and controllable radial force given by

$$\begin{aligned} N &= M \pm 1 \\ \frac{2N}{W} &\notin \mathcal{N} \end{aligned} \tag{13}$$

Note here that the condition for a stable radial force coincides with the '$P \pm 2$' formula presented by Okada, et al. [6] and the control currents also should not be given in phase or out of phase, in the same way as for the motoring currents. Substituting equations (7) and (13) into equation (12), we obtain

$$\begin{aligned} F_x &= \pm\frac{1}{2}WBCkl\sin((Q\pm1)\alpha)\cos\phi \\ F_y &= \frac{1}{2}WBCkl\sin((Q\pm1)\alpha)\sin\phi \end{aligned} \tag{14}$$

where the double signs are aligned with equation (13). Equation (14) proves that the strength and the two dimensional direction of the radial force can be linearly controlled by the magnitude *C* and the phase shift ϕ of the current, respectively. It also reveals that the winding pitch angle to get the maximum radial force is slightly different from that for the maximum torque, i.e. the angle becomes narrower or wider according to the pole pairs of the control current and the sign of *Q*. The radial control force is also independent of the rotational speed of the rotor, which makes it simple to design the radial position controller of the system, not requiring a complex frequency demodulation step. Finally, the torque generated by the radial force currents and the radial force generated by the motoring current should be zero for the decoupled controllability:

$$T^C = \sum_{i=0}^{W-1} rl\int_0^{2\pi} B_R I_i^C D_i\, d\theta = 0 \tag{15}$$

$$F_x^M = -\sum_{i=0}^{W-1} l\int_0^{2\pi} B_R I_i^M D_i \sin\theta\, d\theta = 0 \tag{16}$$

$$F_y^M = \sum_{i=0}^{W-1} l \int_0^{2\pi} B_R I_i^M D_i \cos\theta d\theta = 0 \qquad (17)$$

From equations (15), (16), and (17), we can find it possible to decouple the torque and control force generation, when they hold

$$\frac{2M+1}{W} \notin \mathcal{N}, \quad \frac{2M-1}{W} \notin \mathcal{N} \qquad (18)$$

Consequently, equations (7), (13), and (18) suggest numerous feasible combinations of design parameters, part of which are listed in table 1.

EXPERIMENTAL SETUP

The experimental setup was constructed in upright configuration in order to be free of the gravity effect in the radial direction as shown in Fig. 2. Two eddy-current type proximity probes (PU-05A, AEC) were mounted 90° apart from each other, around the lower rotor disk for non-contact measurement of the rotor position. Figure 3 shows one of the stator disks whose windings are molded and fixed into a disk shaped plastic skeleton. Each rotor disk consists of an iron back yoke, thick permanent magnets and a rim-shaped sensor plane attached around the rotor disk as shown in Fig. 4. The dimensions and materials of rotor and stator are listed in table 2. The design of power amplifier is based on linear power operational amplifier chipsets. It includes a current feedback loop that enables a quick response to the input signal in spite of the phase delay caused by the inductance and large back EMF of the stator windings. The digital control scheme has a simple

TABLE 1: Feasible combinations of design parameters

W	M	N	Q	Phase difference		Winding pitch angle	
				$M\eta$ [rad]	$N\eta$ [rad]	Max. T [rad]	Max. F [rad]
5	1	2	6	$2\pi/5$	$4\pi/5$	$\pi/6$	$\pi/7$
			1			π	$\pi/2$
			-4			$\pi/4$	$\pi/3$
6	1	2	7	$\pi/3$	$2\pi/3$	$\pi/7$	$\pi/8$
			1			π	$\pi/2$
			-5			$\pi/5$	$\pi/4$
	2	1	8	$2\pi/3$	$\pi/3$	$\pi/8$	$\pi/7$
			2			$\pi/2$	π
			-4			$\pi/4$	$\pi/5$
7	1	2	8	$2\pi/7$	$4\pi/7$	$\pi/8$	$\pi/9$
			1			π	$\pi/2$
			-6			$\pi/6$	$\pi/5$
	2	1	9	$4\pi/7$	$2\pi/7$	$\pi/9$	$\pi/8$
			2			$\pi/2$	π
			-5			$\pi/5$	$\pi/6$
	2	3	9	$4\pi/7$	$6\pi/7$	$\pi/9$	$\pi/10$
			2			$\pi/2$	$\pi/3$
			-5			$\pi/5$	$\pi/4$

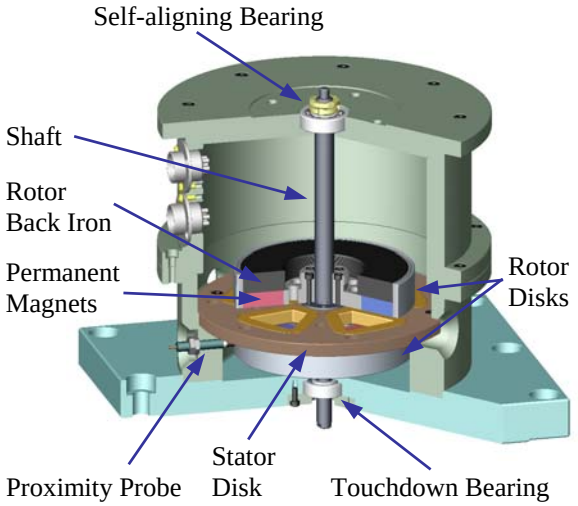

FIGURE 2: Cutaway view of experimental setup

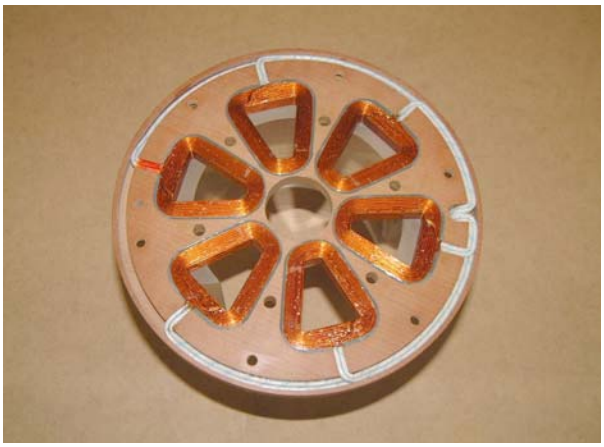

FIGURE 3: Stator with 6 concentrated windings

FIGURE 4: Rotor disks with 8 permanent magnets

TABLE 2: Specifications of rotor and stator

Dimensions	
Outer radius of magnet	50 mm
Inner radius of magnet	25 mm
Magnet thickness	9 mm
Space between magnets	2 mm
Air gap length	9 mm
Number of turns	216
Nominal coil diameter	0.5 mm
Winding width	8 mm
Winding thickness	7.8 mm
Pitch angle	45° for W=5, 36° for W=6
Back iron thickness	9 mm
Rotor disk mass	964 g
Materials	
Magnet	Sintered NdFeB (N-40H)
Rotor disk frame	AL7075
Stator disk frame	Fiber-reinforced bakelite
Rotor back iron	SS400

PD action and modulation with reference to the rotating frequency, implemented on the dSPACE motion control board.

EXPERIMENTS

Prior to the experiment of levitation and rotation, the flux density in the air gap and the static magnetic force were examined. Figure 5 shows the flux density distribution measured by a Gauss meter in the midst of air gap without the stator disk. It well approximates the sinusoidal wave $B(\theta) = 0.78\cos 4\theta$ estimated from the magnetic circuit analysis. Note that the peak value of the flux density is larger than 0.7 T. This smooth distribution results from the large air-gap length and the absence of slot in the stator. The measurement of radial electro-magnetic force along with the current increase is shown in Fig. 6. Here the radial force obtained by unit current is defined as the current stiffness, which is larger than 7 N/A in both cases. This result proves the good linear characteristics of Lorentz force type integrated motor-bearing system as expected. Figure 7 shows the typical time response of the rotor when the

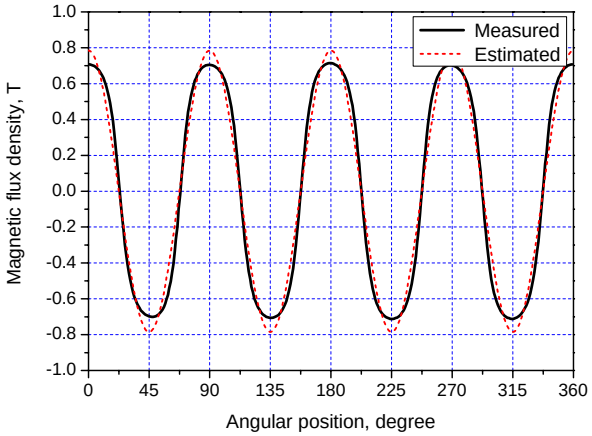

FIGURE 5: Flux density distribution measured in the midst of air gap

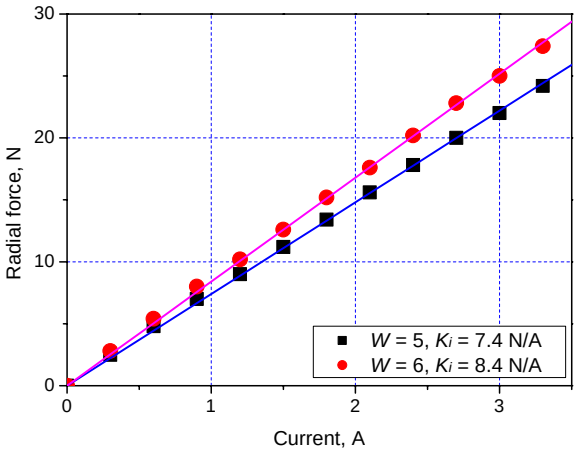

FIGURE 6: Measured current stiffness

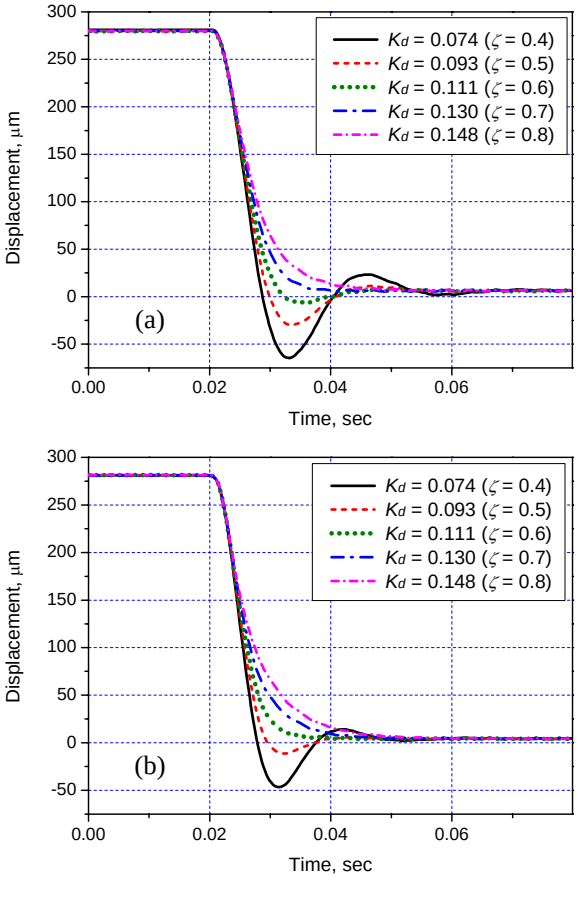

FIGURE 7: Start-up test for (a) W = 5 and (b) W = 6 : K_p = 20, A = 0.5A

regulation control starts at t = 0.02 sec. for the variation of control gains. Owing to no negative stiffness, in fact, any positive control gains are available in the limit of noise level in the sensor signal and the capacity of power amplifier, and the stiffness and damping of the system can be intuitively adjusted through the change of proportional and derivative gains. The curves in the figure show typical responses of the 2nd order system. In a speed up test, the test rotor was successfully operated up to 2300 RPM. The maximum rotational speed is limited mainly by the saturation of back EMF voltage, which is directly proportional to the rotational speed. However, regardless of the control gain changes, the shaft vibration with the amplitude of about 20 μm is observed as the rotational speed increases, as shown in Figs. 8 and 9. The whirling motions are found very complicated, indicating that there exist various high frequency components, up to several times higher than the rotational speed. It is well known that the mechanical runout of sensor target and the mass unbalance of rotor contribute to this kind of oscillation, but this phenomenon is likely to be due to the uneven distribution and higher harmonics of magnetic flux density, which distort the radial force. For instance, the peak located about 50 RPM in Fig. 8 resulted from the interference of the motoring currents with the 3rd harmonics of magnetic flux field. Such undesirable errors, if not large, are inevitable in most of motors. The modeling and reduction scheme of such effects is in progress.

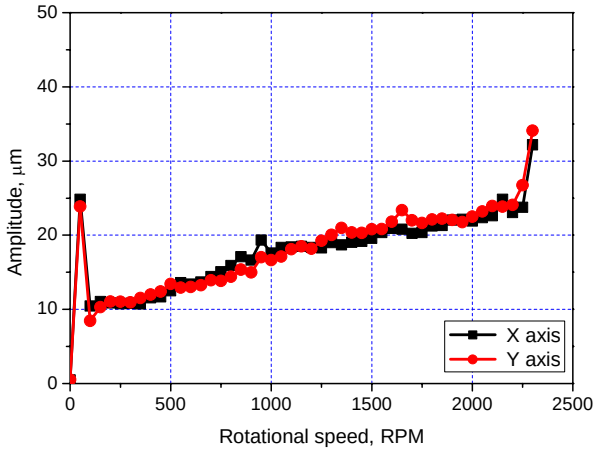

FIGURE 8: Radial response : W = 5, K_p = 20, K_d = 0.148, A = 0.5A

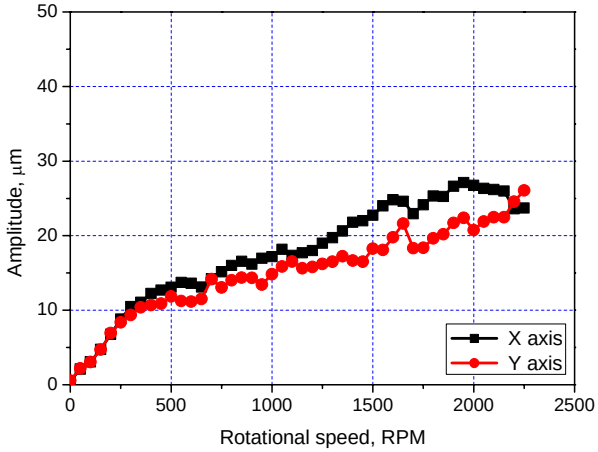

FIGURE 9: Radial response : W = 6, K_p = 40, K_d = 0.157, A = 0.5A

CONCLUSIONS

In this paper, a systematic, comprehensive approach to generation of torque and radial force in integrated motor-bearing systems using Lorentz force is presented. This extended principle can cover the design theories proposed by Okada, et al. [4] and Kim, et al. [5]. It provides a useful guideline to find the most suitable design for a Lorentz force type integrated motor-bearing system, subject to the given design constraints. To verify the proposed scheme, a test rig was made in dual rotor disk configuration using a coreless stator, so that it can be free from the negative stiffness. Finally, the experimental results verified the static and dynamic characteristics and the feasibility of the proposed system.

REFERENCES

1. A. O. Salazar, A. Chiba, and T. Fukao, “A Review of developments in bearingless motors,” *Proc. 7th Int. Symp. Magnetic Bearings*, ETH, Zurich, pp. 335-340, Aug. 2000
2. W. S. Han, C. W. Lee, and Y. Okada, “Design and control of a disk-type integrated motor-bearing system,” *IEEE/ ASME Trans. on Mechatronics*, Vol. 7, No. 1, pp. 15-22, Mar. 2002
3. L. S. Stephens, H. M. Chin, “Robust stability of the Lorentz-type self-bearing servomotor”, *Proc. 8th Int. Symp. Magnetic Bearings*, Mito, Japan, pp. 27-33, Aug. 2002
4. Y. Okada, H. Konishi, H. Kanebako, and C. W. Lee, “Lorentz force type self-bearing motor,” *Proc. 7th Int. Symp. Magnetic Bearings*, ETH, Zurich, pp. 353-358, Aug. 2000
5. S. J. Kim, K. Abe, H. Kanebako, Y. Okada, and C. W. Lee, “A Lorentz force type self-bearing motor with new 4-pole winding configuration,” *Proc. 8th Int. Symp. Magnetic Bearings*, Mito, Japan, pp. 35-40, Aug. 2002
6. Y. Okada, K. Dejima, and T. Ohishi, “Analysis and comparison of PM synchronous motor and induction motor type magnetic bearings,” *IEEE Trans. on Industry Applications*, Vol. 31, No. 5, pp. 1047-1053, 1995